Combustion and Flame 182 (2017) 102–113

Contents lists available at ScienceDirect

Combustion and Flame

journal homepage: www.elsevier.com/locate/combustflame

Multi-channel nanosecond discharge plasma ignition of premixed propane/air under normal and sub-atmospheric pressures

Bing-xuan Lin[a,b], Yun Wu[b,*], Zhi-bo Zhang[a], Zheng Chen[c]

[a] Science and Technology on Plasma Dynamics Laboratory, Air Force Engineering University, Xi'an 710038, China
[b] Science and Technology on Plasma Dynamics Laboratory, Xi'an Jiaotong University, Xi'an 710049, China
[c] SKLTCS, Department of Mechanics and Engineering Science, College of Engineering, Peking University, Beijing 100871, China

ARTICLE INFO

Article history:
Received 23 November 2016
Revised 16 April 2017
Accepted 17 April 2017

Keywords:
Ignition
Multi-channel nanosecond discharge
Ignition kernel
Propane/air
Low pressure

ABSTRACT

Relight of jet engines at high altitude is very difficult due to the relatively low pressure and temperature of inlet air. Currently, advanced ignition technology for high-altitude relight in jet engines is urgently needed. Successful ignition is achieved only when the ignition kernel can propagate outwardly beyond the so-called critical flame initiation radius. At high altitude with low pressure, the critical flame initiation radius becomes large and it cannot be easily reached by the ignition kernel. Therefore, in order to achieve successful ignition at low pressure conditions, large ignition kernel should be generated. In this study, plasma assisted ignition using multi-channel nanosecond discharge (MND) is proposed to induce a large ignition kernel and to achieve successful ignition at low pressures. Ignition experiments for propane/air mixtures at different equivalence ratios ($\Phi = 0.8\sim1.6$) and under normal and sub-atmospheric pressures ($P = 0.3\sim1.0$ bar) were conducted in a constant volume combustion chamber. The performance of three ignition methods, spark discharge, single-channel nanosecond discharge (SND) and MND, were assessed; and the advantages of MND for ignition at sub-atmospheric pressures were demonstrated. The ignition kernel development, ignition probability, minimum ignition energy, and flame development for these three ignition methods (spark, SND and MND) were measured and compared. It was found that compared to spark and SND, MND can generate a much larger ignition kernel with stronger flame wrinkling and has much higher ignition probability, especially at low pressures. Therefore, MND has the advantage in achieving successful ignition at low pressure. Besides, it was shown that though the ignition kernel evolution and ignition probability strongly depend on ignition methods, the subsequent flame propagation is not greatly affected by ignition and there is little change in the flame rise time for different ignition methods.

1. Introduction

Reliable high-altitude relight is crucial for safety and performance of jet engines [1,2]. At high altitude, the pressure and temperature of inlet air to the combustor are relatively low, which results in slow fuel vaporization and chemical reaction [2,3]. Consequently, high-altitude relight become extremely difficult, especially at altitude above 10 km [2,4–7]. Currently, advanced ignition technology for high-altitude relight in jet engines is urgently needed [8,9].

To achieve successful ignition, the amount of energy deposited into the combustible mixture should to be larger than the minimum ignition energy (MIE) [10], otherwise, the resulting ignition kernel eventually decays and it cannot reach the so-called critical flame initiation radius [11–13]. The critical flame initiation radius depends on the Lewis number of the deficient reactant and is proportional to the flame thickness [13]. At higher altitude with lower pressure, the flame thickness becomes larger and so does the critical flame initiation radius. In order to achieve successful ignition, large ignition kernel should be generated at low pressure conditions.

Non-equilibrium plasma is a promising technology for ignition and combustion control [14]. Among different plasma technologies, the nanosecond discharge plasma has recently received great attention and it has been shown to greatly enhance ignition and combustion [14–17]. For examples, Xu et al. [18,19] investigated the development of the ignition kernel induced by nanosecond discharge in lean propane/air mixture. They found that nanosecond discharge with higher frequency or larger number of pulses can effectively reduce the MIE. Sun et al. [20,21] demonstrated that

* Corresponding author.
E-mail address: wuyun1223@126.com (Y. Wu).

http://dx.doi.org/10.1016/j.combustflame.2017.04.022

the nanosecond discharge can make the classical S-curve with separated ignition and extinction limits degenerate to the stretched S-curve without ignition or extinction limit. Starikovskiy et al. [22,23] used nanosecond discharge to control ignition in a rapid compression machine and achieved two-order of magnitude reduction in ignition delay. Lefkowitz et al. [24] examined the effects of nanosecond discharge on ignition using both flame-development visualization and pulsed detonation engine testing platforms. They found that at higher pulse-repetition frequencies (>10 kHz), multiple pulses promote the transition from a ignition kernel to a self-propagating flame and thereby enhance ignition. Besides, though it is not considered in the present study, microwave was also demonstrated to be able to enhance the ignition (e.g., [25–28]). Other examples can be found in the recent review paper by Ju and Sun [14].

However, previous studies mainly focused on single-channel nanosecond discharge (SND) and volumetric nanosecond discharge. Although SND is useful for ignition and combustion enhancement, it is not effective to increase the ignition kernel size at low pressure. The multi-electrode geometries for ignition were investigated in previous studies. Schenk et al. [29] used the multiple tips to distribute the corona directly in a larger ignition volume and thus have better ignition performance. Yu et al [30] used multi-coil power supply to generate distributed spark discharge, which produces faster early flame kernel growth than that of a single high energy spark. Briggs et al. [31] compared several ignition methods including multi-electrode ignition, which shows that a large effective flame kernel and/or a long kernel lifetime is very important for ignition at lean condition.

For nanosecond discharge plasma ignition, the transient nanosecond plasma [32,33] and the nanosecond surface dielectric barrier discharge plasma [34–36] can generate several random discharge channels, which is very useful for ignition. Comparison of transient nanosecond plasma ignition with spark ignition was done, and the effect of electrode geometry (needle to needle, needle to semicircle and rod to ring) on transient plasma induced ignition performance was studied [32,33]. Several fuel-air mixtures ignition using nanosecond surface dielectric barrier discharge plasma was investigated [34–36]. Ignition delay times, energies deposited in the gaseous mixtures and other parameters were analyzed. Three regimes of multi-point ignition were observed: ignition with a few kernels, quasi-uniform ignition along the edge of high voltage electrodes and ignition along the plasma channels.

In this study, a novel method of multi-channel nanosecond discharge (MND) is introduced to increase the ignition kernel size and to achieve successful ignition at low pressure. To the authors' knowledge, MND has not been used for ignition in previous studies. The objectives of this study are to assess the performance of three ignition methods, spark, SND and MND, and to demonstrate the advantages of MND for ignition at sub-atmospheric pressures. Ignition experiments of premixed propane/air mixture at different equivalence ratios and pressures were conducted in a constant volume combustion chamber. The ignition kernel development, ignition probability, minimum ignition energy, and flame development for different ignition methods were measured and compared.

2. Experimental methods

The experimental setup is shown schematically in Fig. 1. Ignition experiments were conducted in a closed cylindrical combustion chamber whose inner diameter is 5 cm and length is 6 cm. The combustion chamber is made of stainless steel. A pair of quartz windows is mounted at the ends of the cylindrical combustion chamber to allow optical access. Propane/air mixture at specified equivalence ratio was first prepared in a premixing chamber and then filled into the combustion chamber. A broad range of the equivalence ratio, $\Phi = 0.8 - 1.6$, was considered. In all experiments, the initial temperature was fixed to be 300 K. Different initial pressures in the range of 0.3–1.0 bar were considered. A 20-kHz pressure transducer (Jcsensor CYG-1102) was used to record the pressure evolution inside the combustion chamber.

As indicated by in Fig. 2(a), a replaceable electrode and its base are placed in the middle of the cylindrical combustion chamber. The electrode holder is made of a nylon insulating material and it separates the electrode from the metal combustion chamber. Figure 2(b) and (c) show two types of electrode assembly which were used to investigate the performance of different ignition methods. The electrode assembly in Fig. 2(b) is referred to as the single-channel nanosecond discharge (SND), which adopts the single channel discharge actuator. For SND, nanosecond discharge is generated between two electrodes with a gap distance of 1 mm. The multi-channel nanosecond discharge (MND) shown in Fig. 2(c) adopts multiple channel discharge actuator. For MND, all the electrodes are on the same vertical plane and the gap distance is 4 mm. Reliable multi-channel nanosecond discharge was obtained through circuit optimization.

Two types of power supply were used respectively for the nanosecond discharge and spark discharge. The nanosecond discharge generator is a FID Technology FPG 20-20NK with input impedance in the range of 200–500 Ω. The discharge frequency is in the range of 0–20 kHz, and its voltage can be varied continuously from 0 to 20 kV. For spark discharge, the electrode assembly is the same as that of SND shown in Fig. 2(b). In order to make SND and MND comparable, the same voltage output control of FID power supply is adopted. The comparison between the SND and MND is done with the same position of voltage regulation knob. The electrical circuit for spark discharge is shown in Fig. 3. It consists of a DC power supply, a resistor, a capacitor and a trigger module. The output voltage range of the DC power supply is 0–10 kV. The capacitor is 10 nF and the resistor is 167 MΩ.

To quantify the ignition energy, the voltage and current signals were measured by a 75-MHz high-voltage probe (Tektronix P6015A) and a 120-MHz current probe (Pearson 6600), respectively. A 1-GHz oscilloscope (Tektronix DPO4014) was used to record these two signals. The ignition kernel propagation was imaged by high-speed schlieren photography. A high-speed CCD camera operated at the frame rate of 40,000 fps and exposure time of 15 µs was used to record these images.

3. Results and discussion

3.1. Comparison between spark and nanosecond discharge in air

Figure 4 shows the voltage and current profiles during a spark discharge in air. It is well known that the spark discharge process consists of three stages: the breakdown stage, the arc stage and the glow stage [37]. During the breakdown stage, the voltage is shown to be around 4.7 kV. A narrow plasma channel appears and the gap impedance decreases rapidly. Consequently, the current increases rapidly and it goes through the channel with little energy loss. During the arc stage, the plasma channel expands rapidly and transforms into a current channel. As shown in Fig. 4, the current reaches the peak value of 318 A at the time around $t = 0.145$ µs, which is followed by oscillating attenuation. The mixture around the plasma channel reaches very high temperature and thereby an ignition kernel is generated. During the glow stage, most of the discharge energy is released though the current and voltage both decrease. The energy loss at the glow stage is much larger than that at the arc stage, which leads to low energy availability for ignition. The total energy of the spark discharge shown in Fig. 4 is 61.6 mJ.

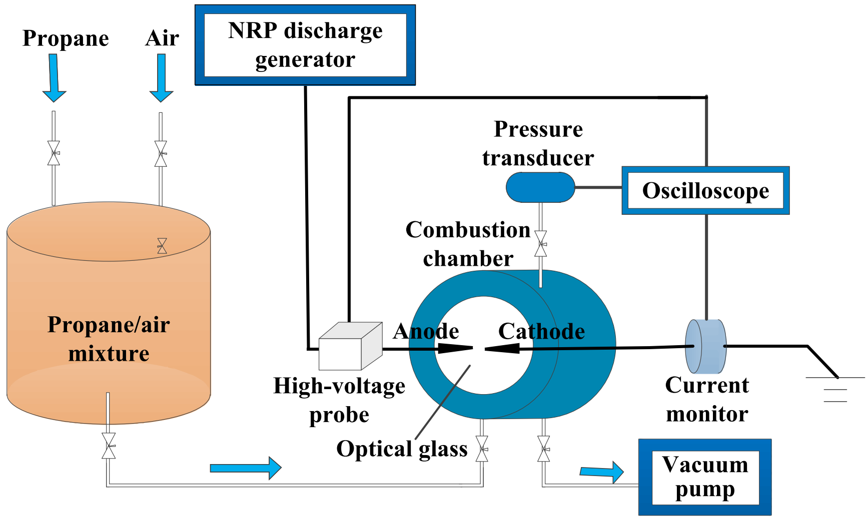

Fig. 1. Schematic of the experimental setup.

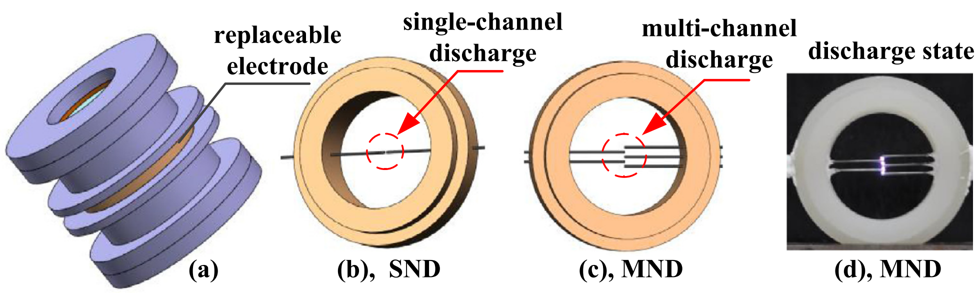

Fig. 2. Electrode assembly: (a), replaceable electrode and its base; (b), single-channel nanosecond discharge (SND); (c), multi-channel nanosecond discharge (MND); (d), discharge stage of MND.

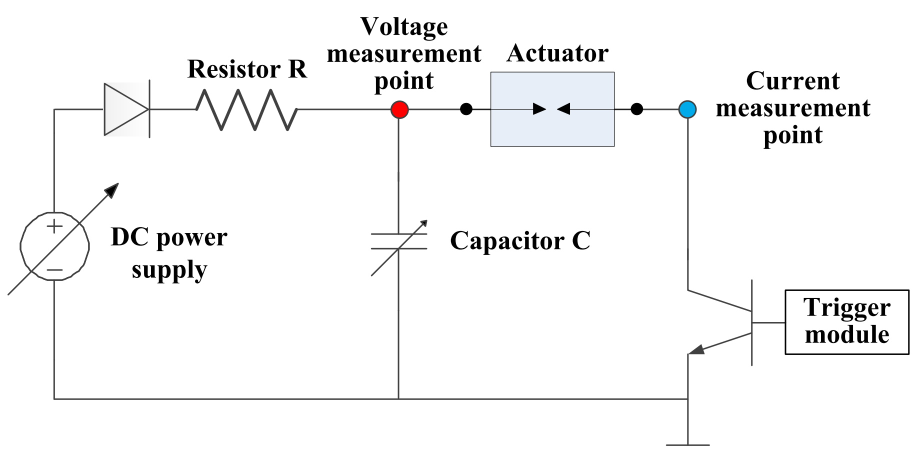

Fig. 3. Electrical circuit for spark discharge.

A fully developed spark channel will transform into an arc with large electrical current. It consumes a large amount of energy and has a weaker kinetic enhancement effect on ignition than nanosecond discharges because of high neutral gas temperature, high electron number density and low electron temperature. To improve the energy efficiency for ignition, the pulse duration can be reduced to a few nanoseconds [37–39]. Consequently, a nanosecond discharge can be used to prevent the streamer-to-arc transition since its energy deposition duration is shorter than the transition time [40,41].

In order to accurately quantify the nanosecond discharge energy, the voltage and current signals need to be synchronized. The conduction current is used to calculate the ignition energy:

$$I_{cond} = I_{total} - I_{disp} \tag{1}$$

$$E = \int_0^t V(t) * I_{cond}(t)dt \tag{2}$$

The synchronization process is carried out at low voltage to ensure that there is no breakdown between the electrodes, thus $I_{cond} = 0$ at low voltage. Consequently, the electrodes can be considered as a pure capacitor, whose displacement current, I_{disp}, can be

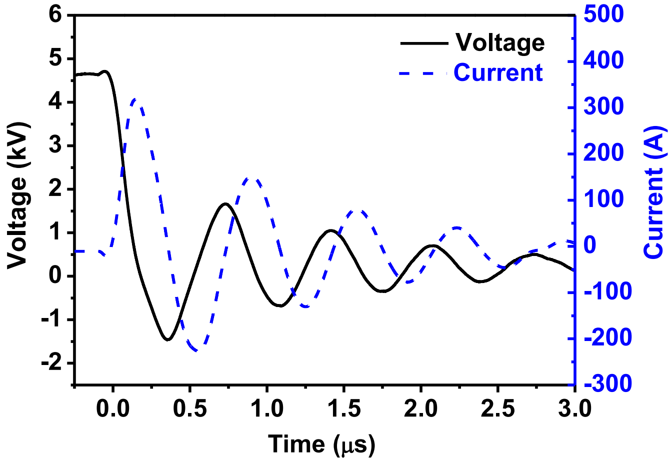

Fig. 4. Voltage and current profiles during a spark discharge in air.

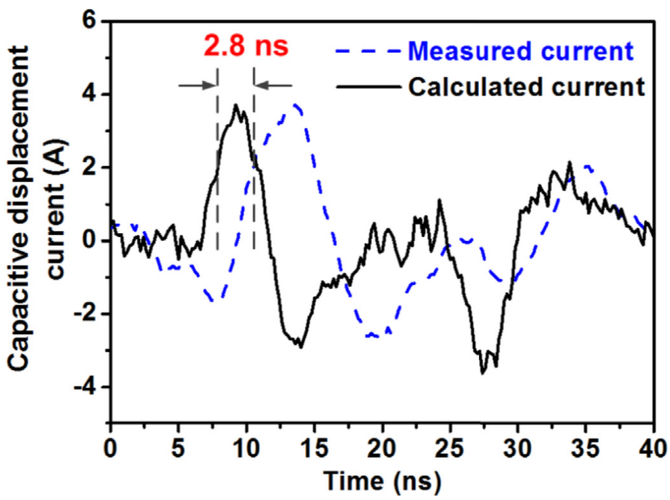

Fig. 5. The time delay between the measured and calculated capacitance displacement currents.

calculated according to the following equation:

$$I_{disp} = C\frac{dV}{dt} \quad (3)$$

where C is the capacitance of the electrode gap and V is the voltage. The capacitance displacement currents from measurement and calculation are compared in Fig. 5. The capacitance of the electrode gap was estimated to be 7.3 pF by matching the measured and calculated currents. The time delay between the measured and calculated currents is shown to be 2.8 ns, which is about 50% of the current rising edge. This time delay was used in all nanosecond discharge experiments.

The FID generator was used to output voltage and current profiles as shown in Fig. 6. The voltage of nanosecond discharge is shown to rise abruptly: it reaches the peak value of 14.3 kV within about 3 ns. The pulse duration is about 10 ns. For high frequency nanosecond discharge, the air plasma impedance during the first pulse is larger than that during the subsequent pulses [18]. The energy of SND discharge is 0.97 mJ for the first breakdown pulse and 0.57 mJ for the subsequent pulses. Similarly, the energy of MND discharge is 1.10 mJ for the first breakdown pulse and 0.64 mJ for the subsequent pulses.

3.2. Ignition kernel development

The ignition kernel development at ambient pressure ranging from 0.3 to 1 bar was investigated for propane/air mixtures. The

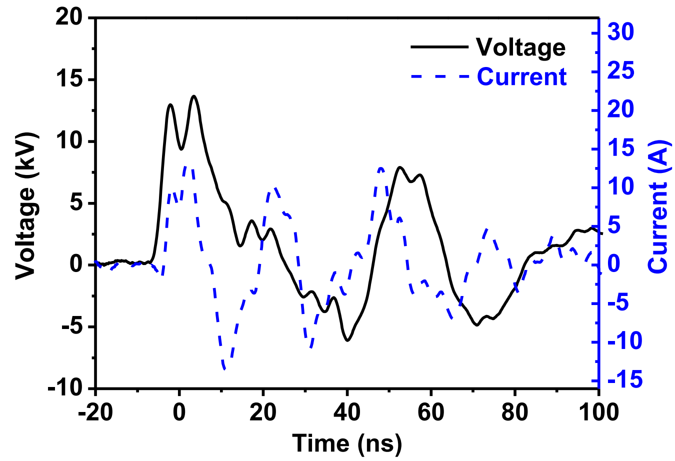

Fig. 6. Synchronized voltage and current profiles during the nanosecond discharge in air.

schlieren images for the ignition kernel development induced by spark, SND (a train of 75 consecutive pulses) and MND (a train of 75 consecutive pulses) are compared in Fig. 7. The ignition kernel is first generated at the center of the discharge channel, and then it evolves into a self-sustained propagating flame under favorable conditions. The evolution of the ignition kernel induced by spark is shown to be similar to that induced by SND. For SND ignition, the kernel growth is mainly induced by the energy deposition during subsequent pulses. since the plasma kernel can sustain about 100 μs [18,42], 67 μs for 15 kHz, the initial weak plasma kernel is not cooled down and is greatly enhanced by the subsequent pulses (i.e., synergetic effects can be induced by multiple pulses). Besides, Fig. 7 also shows that the spherical ignition kernel induced by spark ignition is much smoother that that induced by SND ignition. The flame wrinkling induced by SND can accelerate the propagation of the ignition kernel. Therefore, nanosecond discharge can induce a quickly growing ignition kernel.

Compared to spark and SND ignition, the MND ignition generates a much larger ignition kernel in the early stage as shown in Fig. 7. Besides, compared to SND, MND induces stronger flame wrinkling, resulting faster ignition kernel propagation. Therefore, MND can greatly enhance ignition by generating large and quickly growing ignition kernel.

The above conclusions are further demonstrated by the results in Fig. 8, which shows the ignition kernel development induced by spark, SND and MND in propane/air mixture at sub-atmospheric pressures ($\Phi = 0.8$, $P = 0.75$ bar; and $\Phi = 1.0$, $P = 0.5$ bar). Comparison between Figs. 7 and 8 indicates that MND can further enhance the ignition in leaner propane/air mixture and at lower ambient pressure. Leaner propane/air mixture has larger Lewis number [43]; and flame thickness becomes larger at lower pressure. Consequently, for leaner propane/air mixture at lower pressure, much larger critical flame initiation radius is required and it is much more difficult to generate an ignition kernel which can propagate outwardly beyond the critical flame initiation radius. Since MND is able to create a much larger ignition kernel than spark and SND, it has the advantage in achieving successful ignition more easily in fuel lean propane/air mixture at sub-atmospheric pressures.

3.3. Ignition probability and MIE

The ignition probability, P, is popularly used to quantify the ignition capabilities of different types of discharge. It is defined as the ratio between the number of successful ignition events and the total number of trials. Based on this definition, the total number of trials should be large enough so that it has little influence

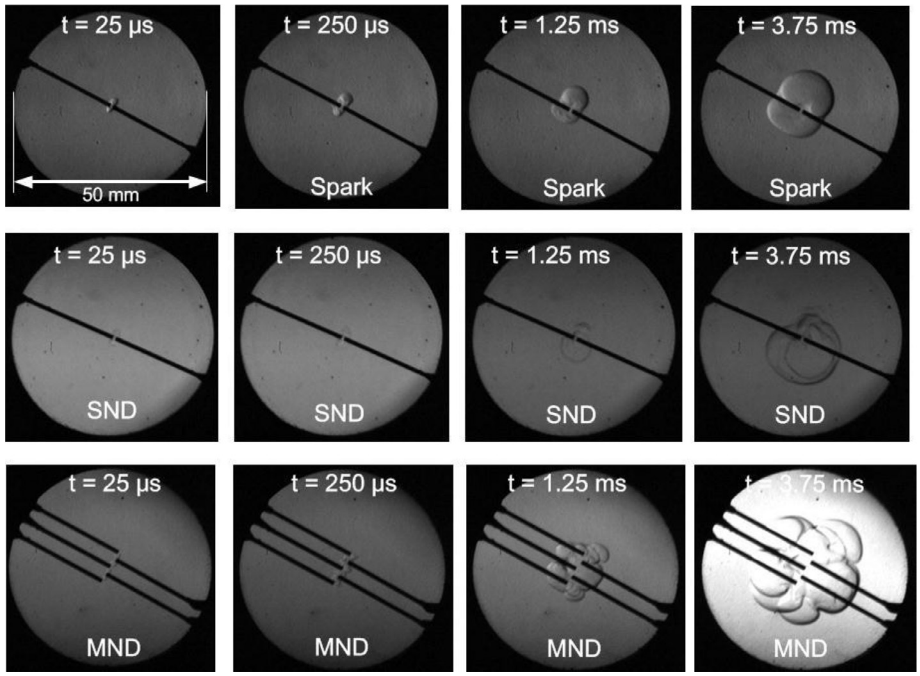

Fig. 7. Development of ignition kernel induced by spark ignition (61.6 mJ, top), SND ignition (15 kHz, 43.15 mJ, middle) and MND ignition (15 kHz, 48.46 mJ, bottom) in stoichiometric propane/air mixture at 1 bar.

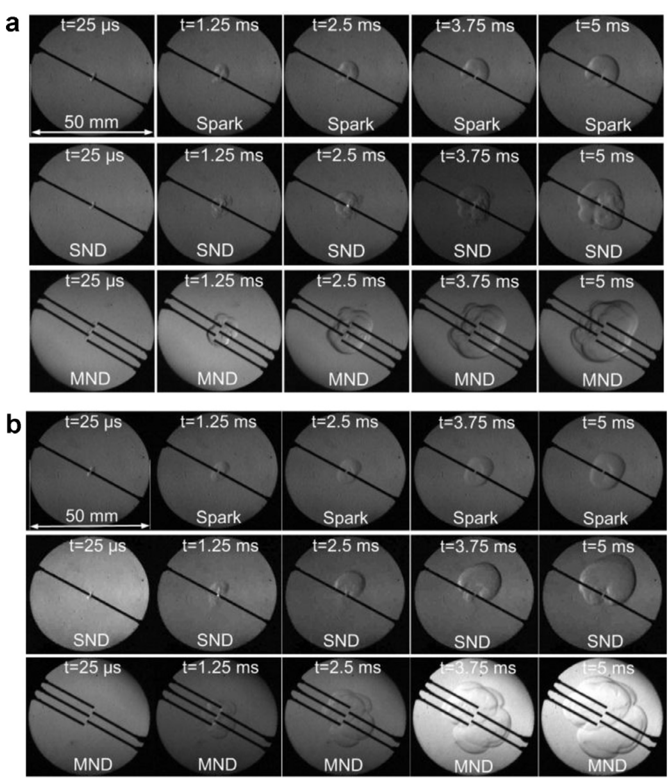

Fig. 8. Ignition kernel development in propane/air: (a), $\Phi = 0.8$ and $P = 0.75$ bar; and (b), $\Phi = 1.0$ and $P = 0.5$ bar, with spark ignition (61.6 mJ), SND ignition (15 kHz, 43.15 mJ) and MND ignition (15 kHz, 48.46 mJ).

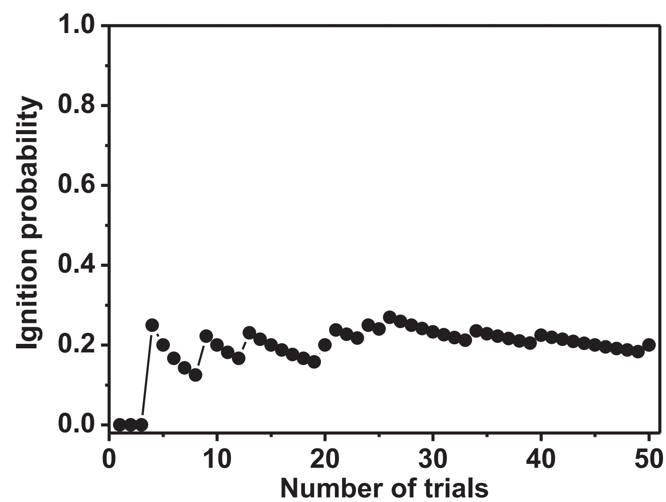

Fig. 9. Ignition probability versus number of trials for SND in stoichiometric propane/air mixture at 1 bar.

on the value of ignition probability. Figure 9 shows the ignition probability as a function of trial number. The mixture is stoichiometric propane/air at 1 bar. SND discharge with a train of 20 pulses (15 kHz, 11.8 mJ in total) was used. It is seen that the ignition probability converges when the number of trials is above 30. In this study, 40 trials were conducted for each condition so that reliable value of ignition probability was reached.

To determine the MIE, the ignition probability P as a function of ignition energy E was fitted by the following equation [44]:

$$P(E) = \frac{1}{1 + e^{-(\beta_0 + \beta_1 E)}} \tag{4}$$

where β_0 and β_1 are fitting parameters. Figure 10 shows the results for stoichiometric propane/air at different pressures. Each experimental data point represents a minimum of 40 trials for SND with the ignition energy in the range from 11.8 mJ (15 kHz, 20 pulses) to 171.4 mJ (15 kHz, 300 pulses). The results in Fig. 10 demonstrate that the experimental data (symbols) at different pressures are well fitted by Eq. (4) (lines).

Similar to previous studies (e.g., [45]), the minimum ignition energy (MIE), E_{MIE}, is defined as the energy corresponding to

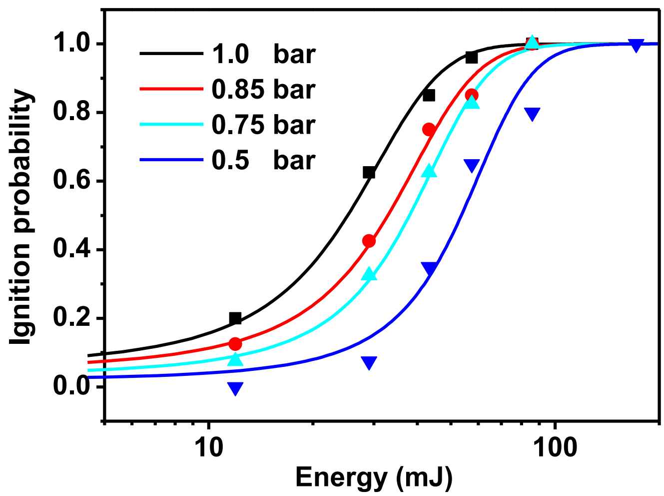

Fig. 10. Ignition probability as a function of SND discharge energy for stoichiometric propane/air mixture at different pressures. The symbols are experimental data and the lines are fitting curves according to Eq. (4).

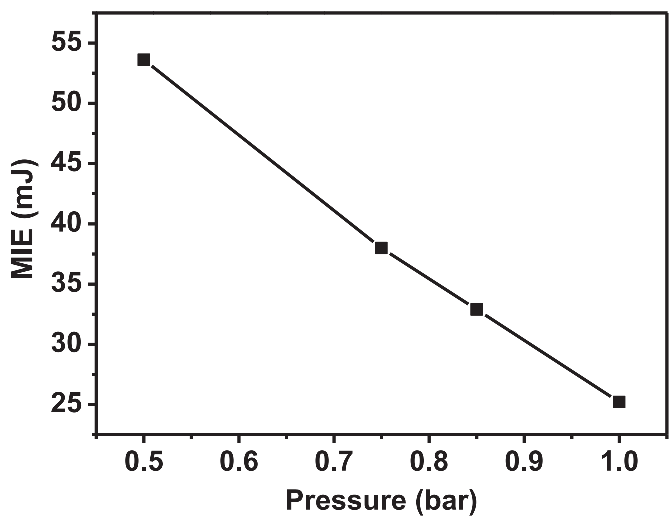

Fig. 11. Minimum ignition energy as a function of the pressure for stoichiometric propane/air mixture ignited by SND.

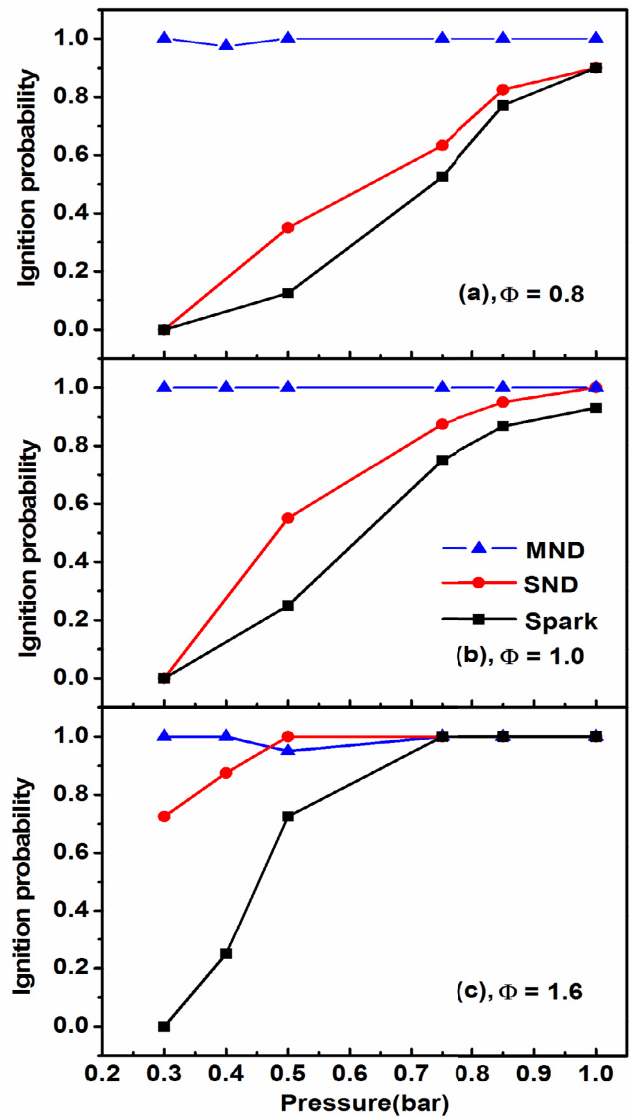

Fig. 12. Ignition probability as a function of pressure for propane/air mixture with the equivalent ratio of 0.8 (a), 1.0 (b) and 1.6 (c). The results are presented for three ignition methods: spark (61.6 mJ), SND (15 kHz, 43.15 mJ) and MND (15 kHz, 48.46 mJ).

ignition probability of 50%. Figure 11 shows the change of the MIE with the ambient pressure for stoichiometric propane/air mixture ignited by SND. As expected, the MIE is shown to increase greatly as the pressure decreases. The MIE at 1.0 bar is 25.2 mJ; while that at 0.5 bar is 53.6 mJ. Therefore, the MIE is increased by more than 100% at sub-atmospheric pressure of 0.5 bar. Similar trend was observed by Zhang et al. [46].

The ignition probability of different ignition methods, spark, SND and MSD, is compared in Fig. 12 for lean, stoichiometric and rich propane/air mixtures at different pressures ranging from 0.3 bar to 1.0 bar. The discharge energy of the spark ignition was fixed to be 61.6 mJ. The FID power supply was controlled to output 75 pulses at 15 kHz. The total ignition energy for SND and MND was 43.15 mJ and 48.46 mJ, respectively. It is observed in Fig. 12 that the ignition probability of both spark and SND ignition drops quickly as the pressure decreases. This is due to the fact mentioned before that ignition becomes more difficult at lower pressure. The ignition probability of SND ignition is higher than that of spark ignition at the same pressure. This indicates that nanosecond discharge helps to achieve successful ignition.

Compared to spark and SND ignition, MND ignition is shown to have the highest ignition probability. Bedsides, it is observed that ignition probability of MND remains nearly constant (close to unity) as the pressure decreases. Figure 12(a) and (b) indicates that at low pressure of 0.3 bar and for fuel lean and stoichiometric mixtures, successful ignition cannot be achieved through spark and SND. However, MND ignition can still maintain nearly 100% ignition probability. Therefore, compared to spark and SND, MND has the advantage of achieving successful ignition at low pressures. Figure 12 also indicates that fuel-lean propane/air mixture is much more difficult to be ignited than fuel-rich mixture at the same low initial pressure. This is due to the facts that the leaner propane/air mixture has larger Lewis number [43] and that the critical ignition radius and MIE both increase monotonically with the Lewis number [11,13].

3.4. Flame development

The effects of different ignition methods on flame development were examined in this subsection. The pressure history inside the

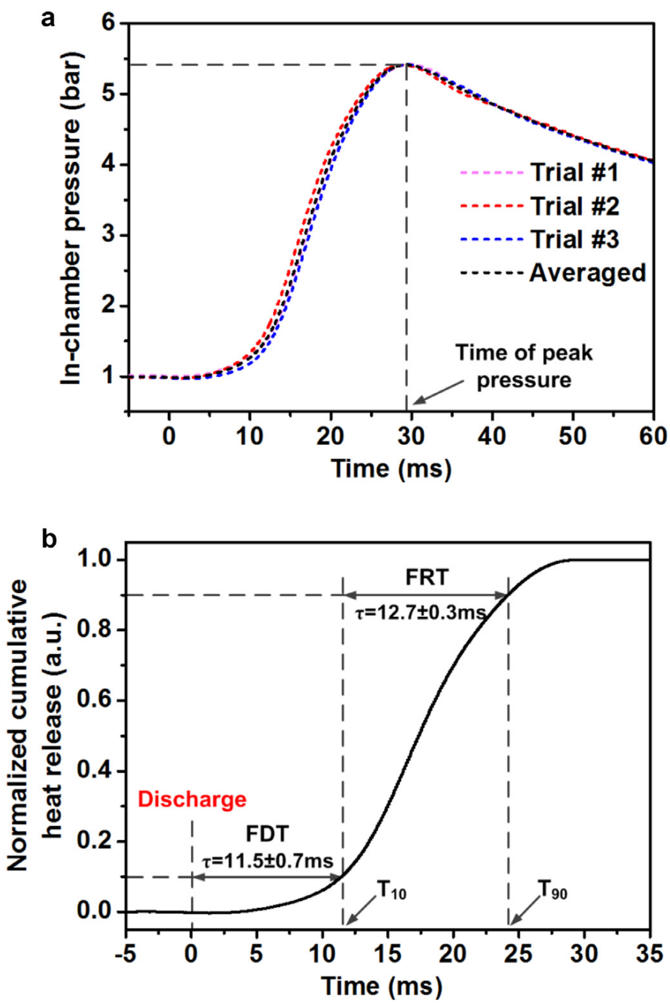

Fig. 13. (a) In-chamber pressure and (b) the normalized cumulative heat release (NCHR) for propane/air ($\Phi = 0.8$ and P = 1 bar) ignited by SND (15 kHz 43.15 mJ).

combustion chamber, $P_{in\text{-}chamber}$, was recorded and an example is shown in Fig. 13(a) for stoichiometric propane/air initially at 1 bar. For each condition, we conducted three trials, based on which the averaged in-chamber pressure history was obtained. Following Hwang et al. [28], we calculated the representative heat release rate (RHRR) and the normalized cumulative heat release (NCHR) according to the following equations:

$$\mathrm{RHRR} = \frac{dP_{in-chamber}}{dt} \tag{5}$$

$$NCHR = \frac{\int_{t_0}^{t} \mathrm{RHRR}\, dt}{\int_{t_0}^{t_{end}} \mathrm{RHRR}\, dt} \tag{6}$$

where t_0 is the time of discharge, and t_{end} is the end of combustion where the measured pressure reaches its peak [28].

To quantify the time duration for the ignition and combustion phases, we used the flame development time (FDT) and flame rise time (FRT) introduced by Hwang et al. [28]. The FDT was defined as the time duration from the start of the ignition command to 10% of the total NCHR [28]; and the FRT was defined as the time duration from 10% to 90% of the NCHR [28]. The schematic of NCHR is presented in Fig. 13(b), which shows that the FDT and FRT are 11.5 ± 0.7 ms and 12.7 ± 0.3 ms, respectively.

The above analysis was conducted for spark, SND and MND ignition; and the combustion phases for different ignition methods were compared. Figure 14 shows the results for stoichiometric

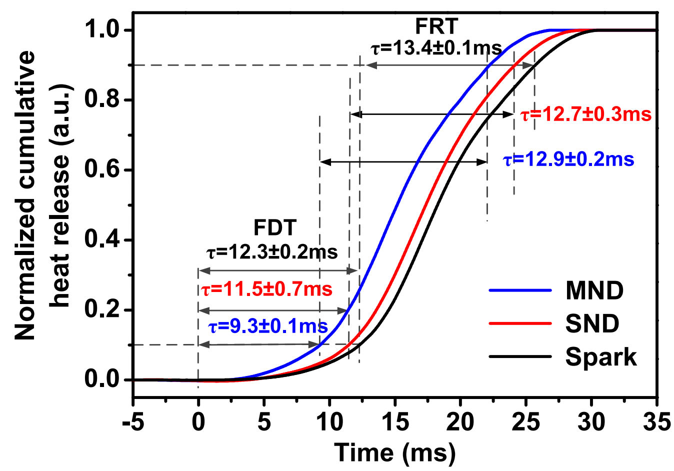

Fig. 14. The NCHR corresponding to by spark ignition (61.6 mJ), SND ignition (15 kHz, 43.15 mJ) and MND ignition (15 kHz, 48.46 mJ) in stoichiometric propane/air initially at 1 bar.

propane/air initially at 1 bar. The FDT and FRT for different ignition methods are presented in Fig. 14. It is observed that the FDT of spark ignition is the largest while that of MND ignition is the smallest. Compared to spark ignition, MND ignition can reduce the FDT by 24%. This confirms the conclusion drawn in Section 3.2 that MND can generate more quickly growing ignition kernel than spark and SND. However, Fig. 14 indicates that there is little change (within 5%) in FRT for different ignition methods. Therefore, the ignition methods only strongly affect the initial ignition kernel development and have little influence on subsequent flame propagation. This is consistent with the conclusion in [47] that ignition has little influence on spherical flame propagation speed when the flame radius reaches some critical value and this conclusion was also obtained by Pancheshnyi et al. [48].

The FDT and FRT results for propane/air at different equivalence ratios ($\Phi = 0.8{\sim}1.6$) and initial pressure of 1 bar are summarized in Fig. 15. It is seen that SND and MND always have lower FDT than spark ignition. Besides, Fig. 15(a) shows that at $\Phi = 0.8$, FDT can be greatly reduced by using SND and MND instead of spark ignition. Since leaner mixture has lower flame propagation speed (due to large Lewis number and high positive stretch rate) and larger critical flame initiation radius, longer FDT is observed in Fig. 15(a) for $\Phi = 0.8$. Richer mixture also has lower flame propagation speed compared to stoichiometric mixture. However, its critical flame radius becomes smaller due to lower Lewis number [47]. Therefore, Fig. 15(a) shows that for fuel-rich mixture, FDT is nearly independent of the equivalence ratio and the influence of ignition methods on FDT becomes relatively weak. This observation is consistent with previous studies about the effect of nanosecond discharge on ignition characteristics [49]. Although SND and MND can reduce the FDT, Fig. 15(b) shows that they have little influence on the FRT except for the case of $\Phi = 0.8$. Similar observation was reported in previous studies by Xu [18], Wolk et al. [27] and Hwang et al. [28], which showed that small energy addition has little influence on subsequent flame propagation. Therefore, the results in Fig. 15 further demonstrate that the ignition methods only strongly affect the initial ignition development and have little influence on subsequent flame propagation.

Figure 16 shows the FDT and FRT for stoichiometric propane/air at different initial pressures ($P = 0.5{-}1$ bar). At the same pressure, the FDT decreases in the order of spark, SND and MND ignition. It is observed that the FDT by MND ignition is about two-thirds of that by spark ignition and that the difference increases as the pressure decreases. Therefore, MND can enhance the ignition by

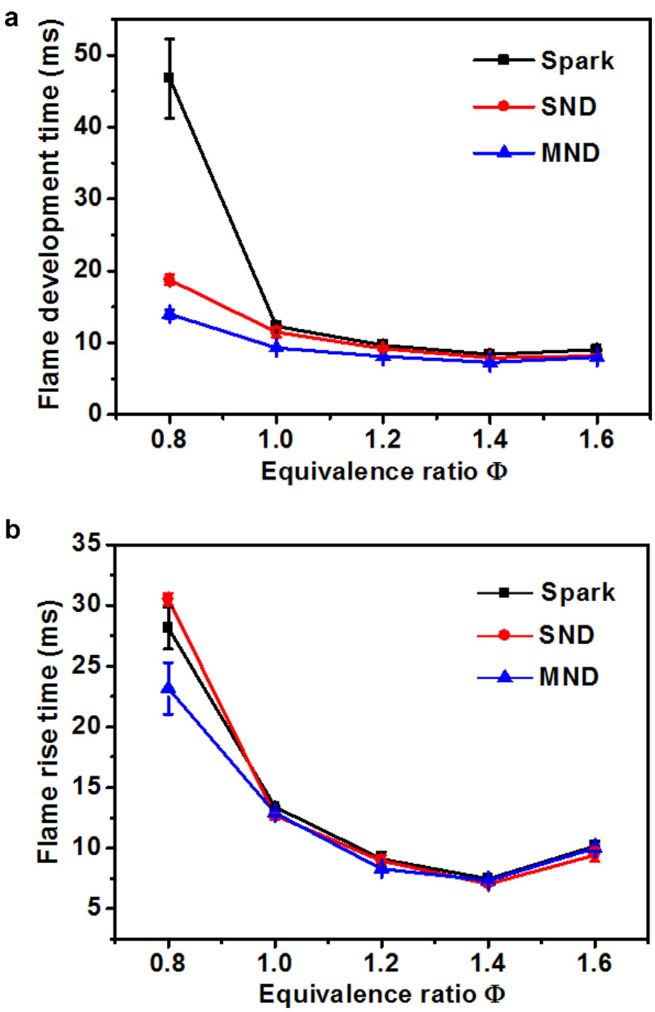

Fig. 15. Change of FDT (a) and FRT (b) by spark (61.6 mJ), SND (15 kHz, 43.15 mJ) and MND (15 kHz, 48.46 mJ) with the equivalence ratio. The ambient pressure is 1.0 bar.

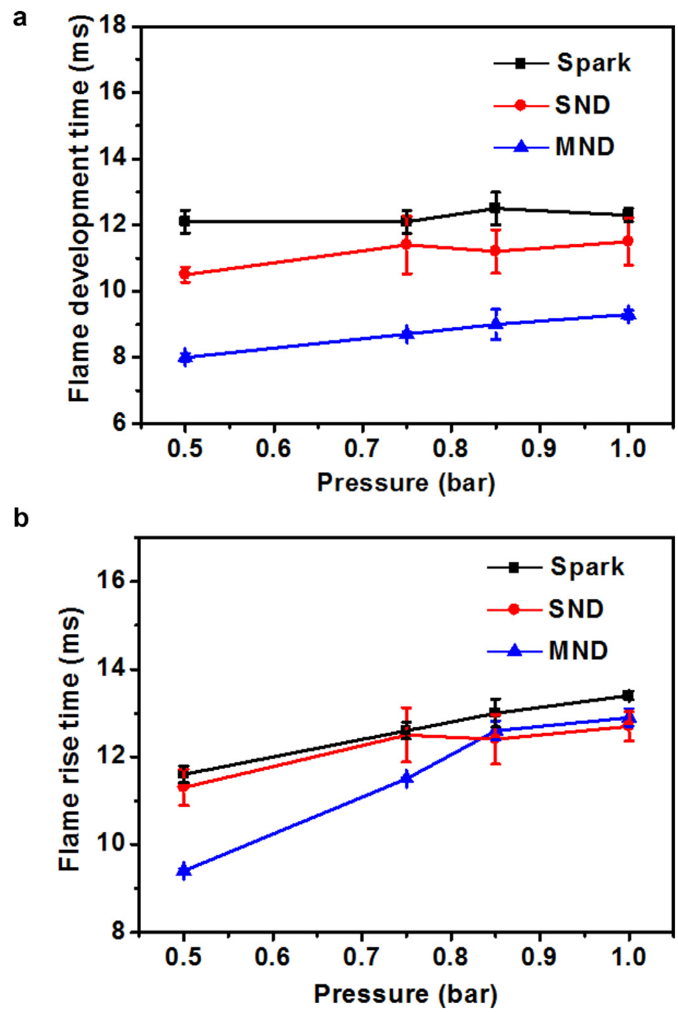

Fig. 16. Change of FDT (a) and FRT (b) by spark (61.6 mJ), SND (15 kHz, 43.15 mJ) and MND (15 kHz, 48.46 mJ) with the ambient pressure.

reducing the FDT at various ambient pressures. As for the FRT, it becomes shorter at lower ambient pressure since the flame propagation speed becomes larger at lower pressure. Figure 16(b) shows that only for $P = 0.5$ and 0.75 bar does MND obviously reduce the FRT. This is due to the facts that the stronger flame wrinkling can induced by MND at lower pressure and that flame wrinkling can also accelerate the subsequent spherical flame propagation.

3.5. Discussion

3.5.1. Comparison of MND with multi-channel spark discharge (MSD)

In order to investigate the advantage of the MND over the same electrode assembly of spark, the experiments of MND and MSD are compared. The ignition kernel development in stoichiometric propane/air mixture at 1 bar is shown in the Fig. 17. Similarly, MSD discharge ignition has a smoother kernel than that of MND discharge. The flame wrinkling induced by nanosecond discharge can accelerate the propagation of the ignition kernel. Thus, the ignition kernel driven by MND increases quickly and catches up the size of flame kernel by MSD within 700 µs.

Compared to MSD discharge, MND discharge combines the advantages of multi-channel and nanosecond discharge. The MND discharge can induce a quickly growing ignition kernel owing to its consecutive pulses and higher energy efficiency. Moreover, the flame wrinkling induced by nanosecond discharge can accelerate the propagation of the ignition kernel. Therefore, MDN can greatly enhance ignition by generating large and quickly growing ignition kernel. Since MND is able to create a much larger ignition kernel than spark SND and MND, it has the advantage in achieving successful ignition more easily in fuel lean propane/air mixture at sub-atmospheric pressures.

Under low pressure, the ignition capability of MSD is lower than that of MND, as shown in Fig. 18. The reason for the ignition capability difference is still unknown, which needs further investigation.

3.5.2. Relevance of measurements at different energies

The calculation of discharge energy of SND and MND is obtained by integrating the voltage and current recorded by the oscilloscope. Due to the extremely steep rising edge, the characteristic of nanosecond discharge is more unstable. Thus, the energy given in this manuscript is the average of multiple measurements. In order to make SND and MND comparable, the same output control of FID power supply is adopted. The comparison between the SND and MND is done with the same knob position, constant output frequency of 15 kHz and the same pulse number of 75.

With the same output control of FID power supply, the MND pulses are 10% more energetic than SND pulses owing to different electrode assemblies. In order to justify the relevance of measurements at different energies, the ignition probabilities of MND using 66 pulses (15 kHz, 42.7 mJ) at 1 bar and 0.5 bar are investigated with stoichiometric propane/air mixture. The result is shown

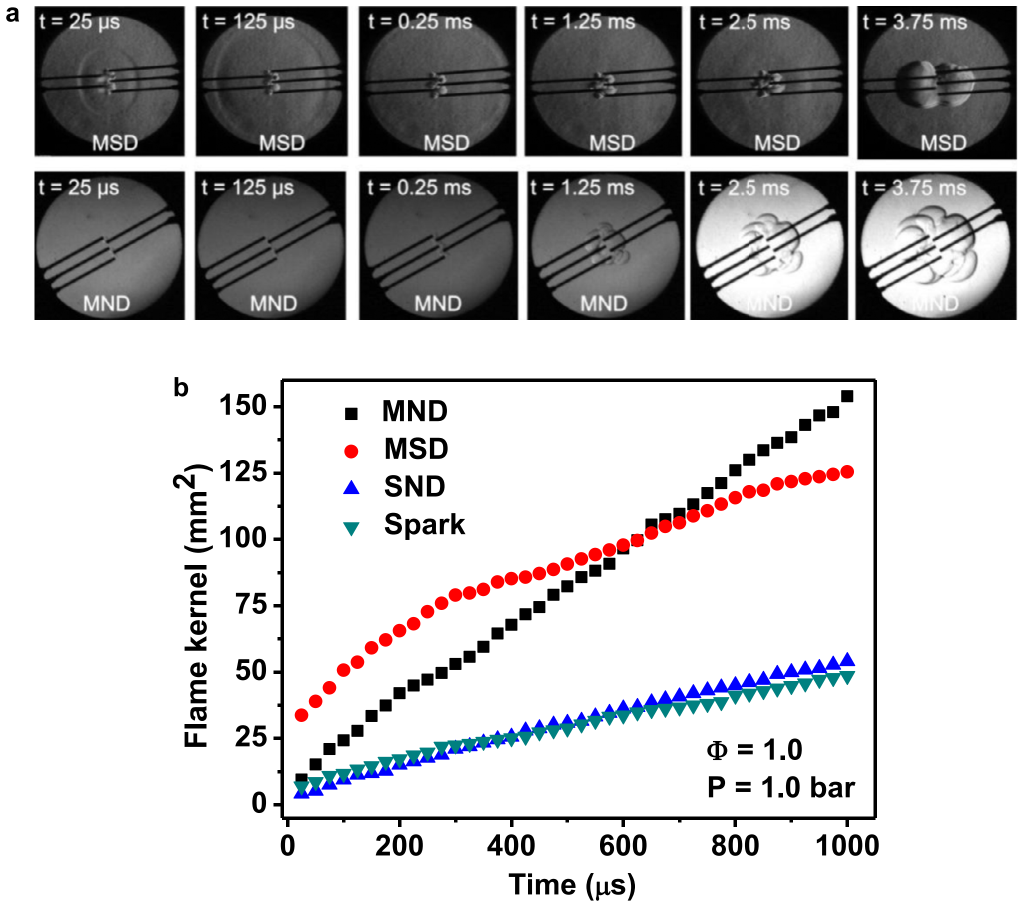

Fig. 17. Development of ignition kernel (a) and ignition kernel size (b) extent vs. time induced by spark (61.6 mJ), SND ignition (15 kHz, 43.15 mJ), MSD (62.23 mJ), and MND ignition (15 kHz, 48.46 mJ) in stoichiometric propane/air mixture at 1 bar.

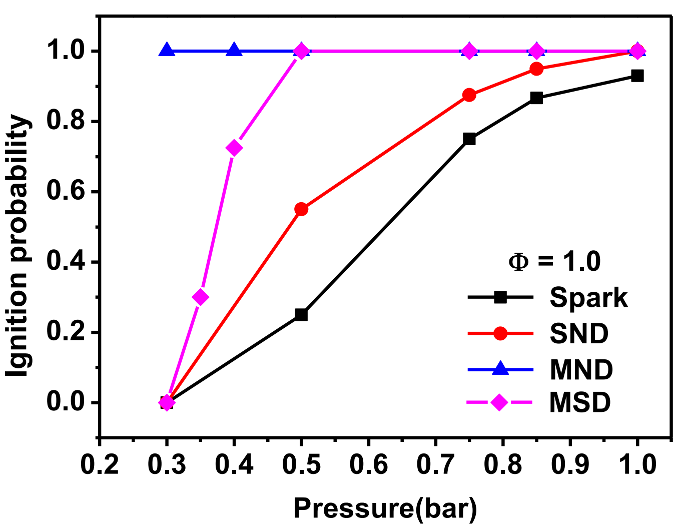

Fig. 18. Ignition probability for stoichiometric propane/air mixture induced by spark (61.6 mJ), SND (15 kHz, 43.15 mJ), MSD (62.23 mJ), and MND (15 kHz, 48.46 mJ).

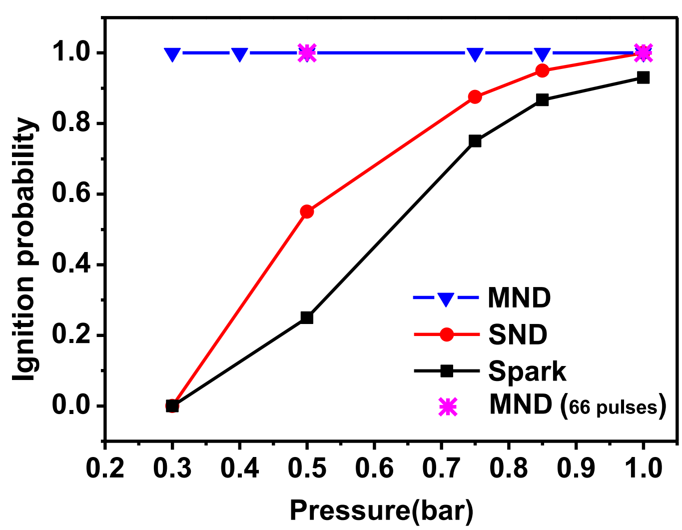

Fig. 19. Ignition probability of four ignition methods: Spark (61.6 mJ), SND (15 kHz, 75 pulses, 43.15 mJ), MND (15 kHz, 75 pulses, 48.46 mJ) and MND (15 kHz, 66 pulses, 42.7 mJ) for stoichiometric propane/air mixture.

in Fig. 19, it can be seen that the ignition probabilities of MND using 66 pulses still keep 100% at 1 bar and 0.5 bar.

The ignition kernel development of MND using 66 pulses (15 kHz, 42.7 mJ) is presented in Fig. 20 with stoichiometric propane/air mixture at 1 bar and 0.5 bar. The ignition kernels driven by MND using 66 pulses are similar to those using 75 pulses at both 1 bar and 0.5 bar. For MND ignition at 1 bar and 0.5 bar, there's almost no obvious influence of the pulses between 66th (4.4 ms) and 75th (5 ms) on the ignition.

3.5.3. Comparison of MND and SND with 4 mm gap

The ignition driven by SND with a 4 mm gap has been done to compare with MND. The ignition probability of different

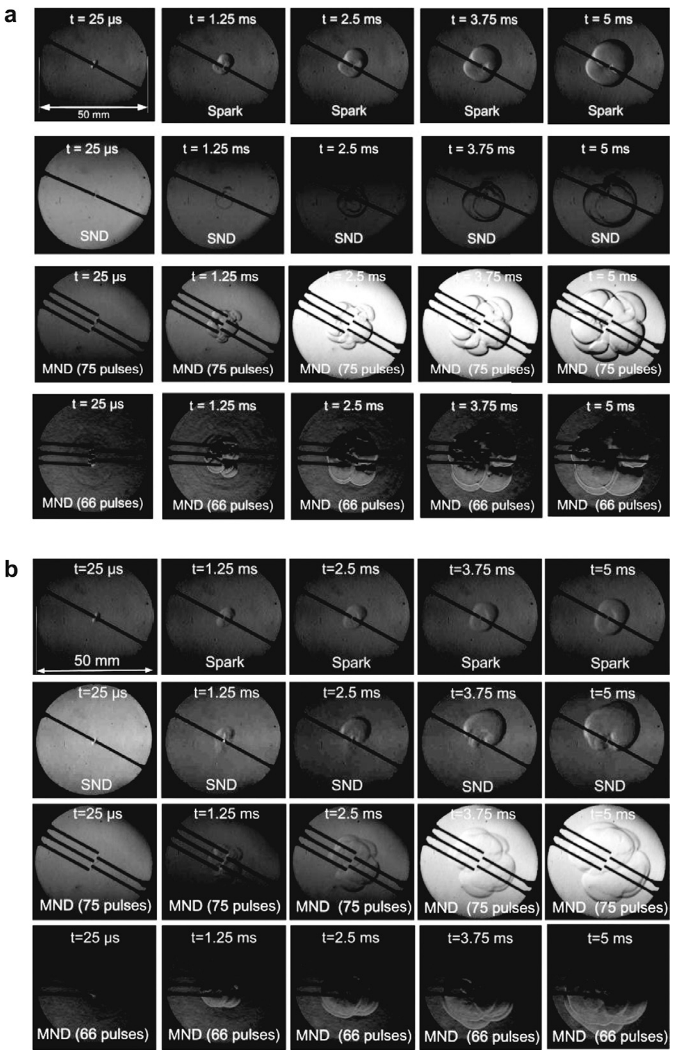

Fig. 20. Ignition kernel development in stoichiometric propane/air mixture: (a), P = 1 bar; and (b) $P = 0.5$ bar, with Spark (61.6 mJ), SND (15 kHz, 75 pulses, 43.15 mJ), MND (15 kHz, 75 pulses, 48.46 mJ) and MND (15 kHz, 66 pulses, 42.7 mJ).

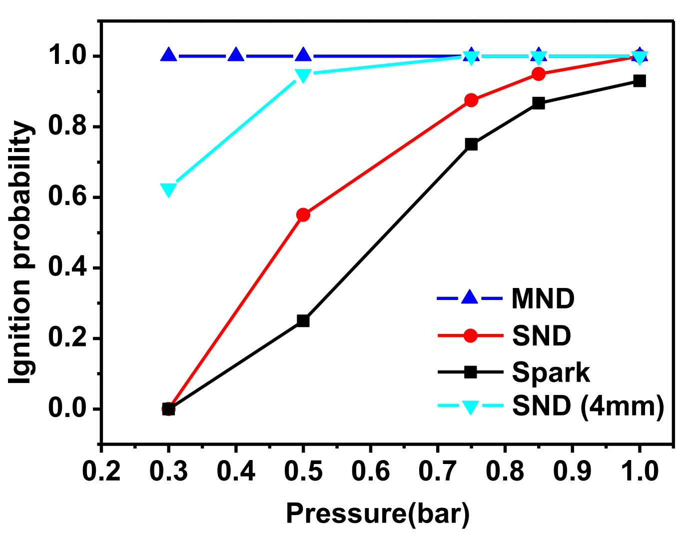

Fig. 21. Ignition probability of four ignition methods: Spark (61.6 mJ), SND (1 mm, 15 kHz, 75 pulses, 43.15 mJ), SND (4 mm, 15 kHz, 75 pulses, 46.62 mJ) and MND (15 kHz, 75 pulses, 48.46 mJ) for stoichiometric propane/air mixture.

ignition methods, spark, SND (1 mm), SND (4 mm) and MND is compared in Fig. 21 for stoichiometric propane/air mixtures at different pressures. The energy of SND (4 mm) discharge is 1.48 mJ for the first breakdown pulse and 0.61 mJ for the subsequent pulses and 46.62 mJ in total. It is observed in Fig. 21 that the ignition probability of SND (4 mm) ignition is higher than that of SND

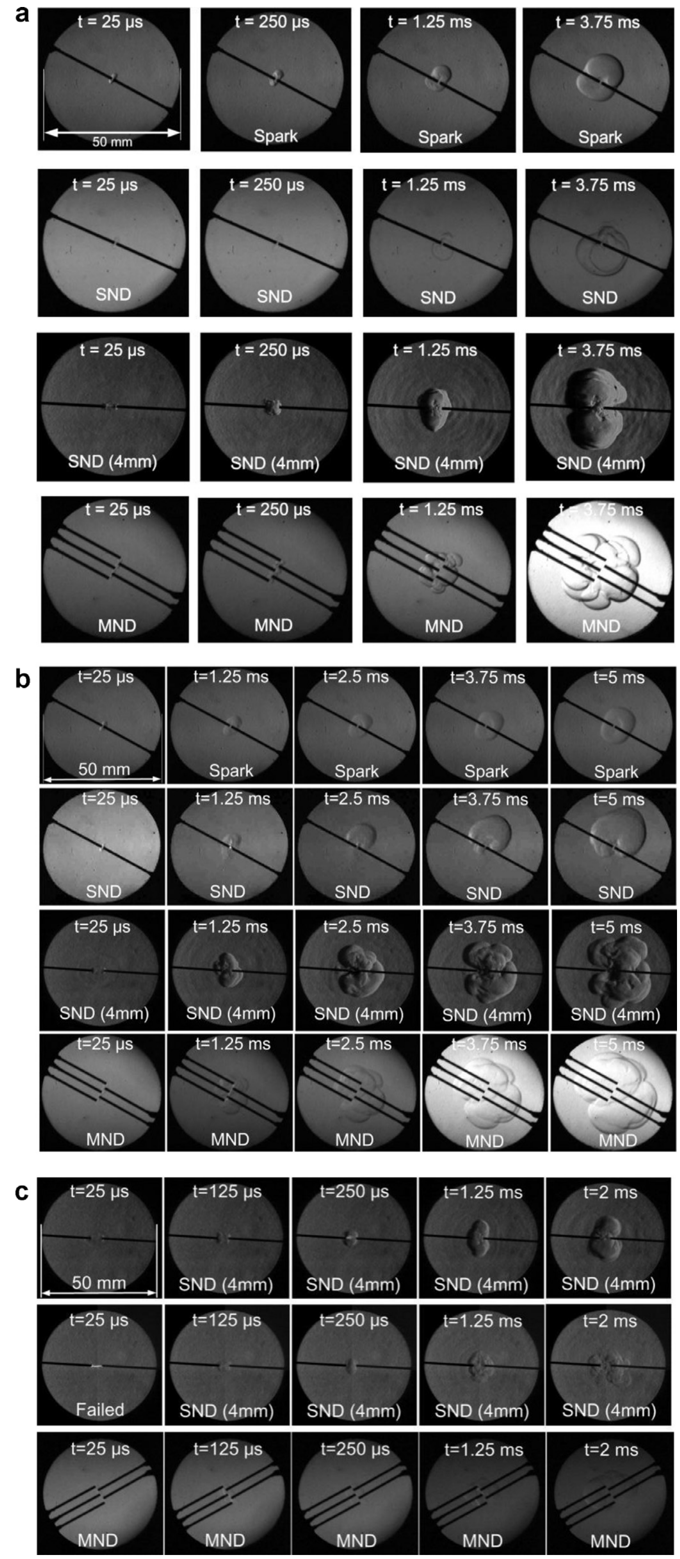

Fig. 22. Ignition kernel development in stoichiometric propane/air mixture: (a), $P = 1$ bar; (b) $P = 0.5$ bar; and (c) $P = 0.3$ bar, with Spark (61.6 mJ), SND (1 mm, 15 kHz, 43.15 mJ), SND (4 mm, 15 kHz, 46.62 mJ) and MND (15 kHz, 48.46 mJ).

(1 mm) at the same pressure. The ignition probability of SND with both 4 mm gap and 1 mm gap drops as the pressure decreases.

The ignition kernel development of Spark (61.6 mJ), SND (1 mm, 15 kHz, 43.15 mJ), SND (4 mm, 15 kHz, 46.62 mJ) and MND (15 kHz, 48.46 mJ) is presented in Fig. 22 with stoichiometric propane/air mixture at 1 bar, 0.5 bar and 0.3 bar. The ignition kernel driven by SND with a 4 mm gap is much larger than that of SND with a 1 mm gap at the same time. A larger initial flame kernel is formed among the long discharge channel. Compared to SND with a 4 mm gap, the MND ignition still generates a larger ignition kernel in the early stage especially at low pressure. As shown in Fig. 22(c), a smaller ignition kernel induced by SND with a 4 mm gap leads to failed ignition. Besides, MND induces much stronger flame wrinkling than SND with a 4 mm gap owing to flow turbulence.

The experimental results indicate that longer gap discharge means larger plasma volume which helps to achieve successful ignition. However, ignition of SND with a 4 mm gap still becomes more difficult at lower pressure. The intricate geometry of MND produces flow turbulence which causes flame wrinkling and accelerates flame propagation at early stage. Moreover, isolation of breakdown stage from discharge process for MND seems to improve the energy utilization efficiency. It should be noted that the breakdown voltage of SND with a 4 mm gap become higher than that with 1 mm gap. It means that successful discharge at low pressure maybe not easily obtained at high pressure especially for engine combustor. The advantage of MND is achieving larger plasma volume with relatively lower breakdown voltage compared to the voltage for single long gap discharge.

4. Conclusions

Multi-channel nanosecond discharge (MND) is proposed to increase the ignition kernel size and to achieve successful ignition at low pressure. Ignition experiments for propane/air mixture at different equivalence ratios ($\Phi = 0.8$–1.6) and pressures ($P = 0.3$–1.0 bar) were conducted. The performance of three ignition methods, spark, SND and MND, were compared and the advantages of MND for ignition at sub-atmospheric pressures were demonstrated. The main conclusions are:

(1) Compared to fully developed spark discharge, the nanosecond discharge has higher energy efficiency for ignition since it releases energy over a few nanoseconds (which is shorter than the transition time to arc) and prevents the streamer-to-arc transition. Compared to spark and SND ignition, the MND ignition generates a much larger ignition kernel. Besides, the ignition kernel induced by MND has strong flame wrinkling which accelerates its propagation. Since MND is able to create a much larger ignition kernel than the spark and SND, it helps to achieve successful ignition more easily, especially at low pressures.

(2) At lower pressure and for leaner propane/air mixture, the critical flame initiation radius becomes larger and thereby ignition becomes more difficult. The ignition probabilities of spark discharge and SND drop quickly with the decrease of pressure and equivalence ratio. Compared to spark and SND ignition, MND ignition has much higher ignition probability, which remains nearly constant as the pressure decreases. Therefore, MND has the advantage in achieving successful ignition in fuel-lean mixture at low pressure.

(3) The influence of different ignition methods on flame development time (FDT) and the flame rise time (FRT) were examined. The FDT of spark ignition is the largest while that of MND ignition is the smallest. This is because MND can generate larger and more quickly growing ignition kernel than spark and SND. However, there is litter change in FRT for different ignition methods, indicating the subsequent flame propagation is not strongly influenced by ignition.

Acknowledgment

This work is supported by the National Natural Science Foundation of China (NSFC) (Nos. 91541120, 51522606, 51336011, 91641204).

References

[1] T. Mosbach, R. Sadanandan, W. Meier, R. Eggels, Experimental analysis of altitude relight under realistic conditions using laser and high-speed video techniques, GT2010-22625, ASME.
[2] A.H. Lefebrave, Gas turbine combustion, 2nd ed., Taylor & Francis, Philadelphia, PA, USA, 1999.
[3] W. Sun, Y. Ju, Nonequilibrium plasma-assistant combustion: a review of recent progress, J. Plasma Fusion Res. 89 (2013) 208–219.
[4] D.W. Naegeli, L.G. Dodge, Ignition study in a gas turbine combustor, Combust. Sci. Technol. 80 (1991) 165–184.
[5] S. Correa, A review of NOx formation under gas-turbine combustion conditions, Combust. Sci. Technol. 87 (1993) 329–362.
[6] G. Pucher, G. Wang, M. Bardon, D. Gardiner, A. Namet-Allah, A. Benaissa, Enhanced ignition systems for aircraft altitude relight, 48th Annual Conference of the Canadian Aeronautics and Space Institute, 48 (2001), pp. 611–620.
[7] G. Pucher, W.D. Allan, Turbine fuel ignition and combustion facility for extremely low temperature conditions, GT2004-53620 ASME.
[8] R.W. Read, Experimental investigations into high altitude relight of a gas turbine, (Ph.D. thesis), University of Cambridge, Cambridge, 2008.
[9] R.W. Read, Relight imaging at low temperature low pressure conditions, AIAA Paper. 2008-957 AIAA.
[10] B. Lewis, G.V. Elbe, Combustion, flames, and explosions of gases, 3rd ed., Academic Press, 1987.
[11] Z. Chen, Y. Ju, Theoretical analysis of the evolution from ignition kernel to flame ball and planar flame, Combust. Theory Model. 11 (2007) 427–453.
[12] A.P. Kelley, G. Jomaas, C.K. Law, Critical radius for sustained propagation of spark-ignited spherical flames, Combust. Flame 156 (2009) 1006–1013.
[13] Z. Chen, M.P. Burke, Y. Ju, On the critical flame radius and minimum ignition energy for spherical flame initiation, Proc. Combust. Inst. 33 (2011) 1219–1226.
[14] Y. Ju, W. Sun, Plasma assisted combustion: Progress, challenges, and opportunities, Combust Flame 162 (2015) 529–532.
[15] S.M. Starikovskaia, Plasma-assisted ignition and combustion: nanosecond discharges and development of kinetic mechanisms, J. Phys. D Appl. Phys. 47 (2014) 353001.
[16] A.Y. Starikovskii, Plasma-supported combustion, Proc. Combust. Inst. 30 (2005) 2405–2417.
[17] W. Sun, M. Uddi, S.H. Won, T. Ombrelleo, C. Carter, Y. Ju, Kinetic effects of non-equilibrium plasma-assisted methane oxidation on diffusion flame extinction limits, Combust. Flame 159 (2012) 221–229.
[18] D. Xu, Thermal and hydrodynamic effects of nanosecond discharges in air and application to plasma-assisted combustion, (Ph.D. thesis), University of Ecole Centrale, Paris, 2014.
[19] D. Xu, D.A. Lacoste, C.O Laux, Schlieren imaging of shock-wave formation induced by ultrafast heating of a nanosecond repetitively pulsed discharge in air, IEEE Trans. Plasma Sci. 42 (2014) 2350–2351.
[20] W. Sun, T. Ombrello, S.H. Won, C. Carter, Y. Ju, Direct ignition and S-curve transition by in situ nanosecond pulsed discharge in methane/oxygen/helium counter-flow flame, Proc. Combust. Inst. 34 (2013) 847–855.
[21] W. Sun, S.H. Won, Y. Ju, In situ plasma activated low temperature chemistry and the S-curve transition in DME/oxygen/helium mixture, Combust. Flame 161 (2014) 2054–2063.
[22] A.Y. Starikovskiy, A. Rakitin, G. Correale, A. Nikipelov, T. Urushihara, T. Shiraishi, Ignition of hydrocarbon-air mixtures with non-equilibrium plasma at elevated pressures, AIAA Paper. 2012-0828, AIAA.
[23] A.Y. Starikovskiy, N. Aleksandrov, Plasma assisted ignition and combustion, Prog. Energy Combust. Sci. 39 (2013) 61–110.
[24] J.K. Lefkowitz, P. Guo, T. Ombrello, S.H. Won, C.A. Stevens, J.L. Hoke, F. Schauer, Y. Ju, Schlieren imaging and pulsed detonation engine testing of ignition by a nanosecond repetitively pulsed discharge, Combust. Flame 162 (2015) 2496–2507.
[25] Y. Ikeda, A. Nishiyama, M. Kaneko, Microwave enhanced ignition process for fuel mixture at elevated pressure of 1 MPa, AIAA paper. 2009-223, AIAA.
[26] Y. Ikeda, A. Moon, M. Kaneko, Development of microwave-enhanced spark induced breakdown spectroscopy, Appl. Opt. 49 (2010) 2471–2477.
[27] B. Wolk, A. DeFilippo, J.Y. Chen, R. Dibble, A. Nishiyama, Y. Ikeda, Enhancement of flame development by microwave-assisted spark ignition in constant volume combustion chamber, Combust. Flame 160 (2013) 1225–1234.
[28] J. Hwang, C. Bae, J. Park, W. Choe, J. Cha, S. Woo, Microwave-assisted plasma ignition in a constant volume combustion chamber, Combust. Flame 167 (2016) 86–96.
[29] A. Schenk, G. Rixecker, S. Bohne, The corona ignition system ecoflash: new results with cng engines and effects of engine-specific boundary conditions, 2nd International Conference on Ignition Systems for Gasoline Engines (2014).

[30] S. Yu, K. Xie, Q. Tan, M. Wang, M. Zheng, Ignition improvement of premixed methane-air mixtures by distributed spark discharge, SAE paper 2015-01-1889, SAE
[31] T. Briggs, T. Alger, B. Mangold, Advanced ignition systems evaluations for high-dilution SI engines, SAE Int. J. Engines 7 (2014), doi:10.4271/2014-01-2625.
[32] D. Singleton, S.J. Pendleton, M.A. Gundersen, The role of non-thermal transient plasma for enhanced flame ignition in C2H4-air, J. Phys. D Appl. Phys. 44 (2011) 022001 (6pp).
[33] B. Shukla, V. Gururajan, K. Eisazadeh-Far, B. Windom, D. Singleton, M.A. Gundersen, F.N. Egolfopoulos, Effects of electrode geometry on transient plasma induced ignition, J. Phys. D Appl. Phys. 46 (2013) 205201 9pp.
[34] E.M. Anokhin, D.N. Kuzmenko, S.V. Kindysheva, V.R. Soloviev, N.L. Aleksandrov, Ignition of hydrocarbon: air mixtures by a nanosecond surface dielectric barrier discharge, Plasma Sources Sci. Technol. 24 (2015) 045014 (13pp).
[35] M.A. Boumehdi, S.A. Stepanyan, P. Desgroux, G. Vanhove, S.M. Starikovskaia, Ignition of methane- and n-butane-containing mixtures at high pressures by pulsed nanosecond discharge, Combust Flame 162 (2015) 1336–1349.
[36] S.A. Shcherbanev, N.A. Popov, S.M. Starikovskaia, Multi-point ignition of hydrogen/air mixtures with single pulsed nanosecond surface dielectric barrier discharge, 54th AIAA Aerospace Sciences Meeting on Morphology of the discharge at elevated pressures (2016).
[37] R. Maly, M. Vogel, Initiation and propagation of flame fronts in lean CH4-air mixtures by the three modes of the ignition spark, Symp. (Int.) Combust. 17 (1979) 821–831.
[38] G. Ziegler, E. Wagner, R. Maly, Ignition of lean methane-air mixtures by high pressure glow and arc discharges, Symp. (Int.) Combust. 20 (1985) 1817–1824.
[39] R. Modien, M. Checkel, J. Dale, The effect of enhanced ignition systems on early flame development in quiescent and turbulent conditions, SAE Technical Paper No. 910564, SAE, 1991.
[40] Z. Machala, D.Z. Pai, M. Janda, C.O. Laux, Atmospheric pressure nanosecond pulsed discharge plasmas in low temperature plasma technology: methods and applications, in: P. Chu, X. Lu (Eds.), Taylor & Francis, USA, 2014.
[41] D.Z. Pai, D.A. Lacoste, C.O. Laux, Transitions between corona, glow, and spark regimes of nanosecond repetitively pulsed discharges in air at atmospheric pressure, J. Appl. Phys. 107 (2010) 093303.
[42] D. Xu, M.N. Shneider, D.A. Lacoste, C.O. Laux, Thermal and hydrodynamic effects of nanosecond discharges in atmospheric pressure air, J. Phys. D Appl. Phys. 47 (2014) 235202 (13pp).
[43] C.K. Law, Combustion physics, Cambridge University, 2006.
[44] S.P. Moffett, S.G. Bhanderi, F.E. Shepherd, E. Kwon, Investigation of statistical nature of spark ignition, 2007 Fall Meeting of the Western States Section of the Combustion Institute (2007) Paper 07F-42.
[45] Y. Ko, R. Anderson, V. Arpaci, Spark ignition of propane-air mixtures near the minimum ignition energy: Part I. An experimental study, Combust. Flame 83 (1991) 75–87.
[46] W. Zhang, X. Gou, Z. Chen, Effects of water vapor dilution on the minimum ignition energy of methane, n-butane and n-decane at normal and reduced pressures, Fuel 187 (2017) 111–116.
[47] Z. Chen, M.P. Burke, Y. Ju, Effects of Lewis number and ignition energy on the determination of laminar flame speed using propagating spherical flames, Proc. Combust. Inst. 32 (2009) 1253–1260.
[48] S.V. Pancheshnyi, D.A. Lacoste, A. Bourdon, C.O. Laux, Ignition of propane–air mixtures by a repetitively pulsed nanosecond discharge, IEEE Trans. Plasma Sci. 34 (2006) 2478–2487.
[49] I.N. Kosarev, A.I. Pakhomov, S.V. Kindysheva, E.M. Anokhin, N.L. Aleksandrov, Nanosecond discharge ignition in acetylene-containing mixtures, Plasma Sources Sci. Technol. 22 (2013) 045018.